In this issue:

Observations from SALT
SARAO joins Ceph Foundation
Mars imaging with 13-inch Boyden Refractor
Fireball Observations
July 27 2018 Lunar Eclipse
Observing an Exoplanet Transit

Cover Photo: Clyde Foster ASSA, Dawid van Jaarsveld UFS with the 13-inch Boyden Refractor of 1887 by Alvan Clark.

News Note: SALT chases hypervelocity stars

The Southern African Large Telescope (SALT) was recently involved in the identification of a hypervelocity star, flung across the galaxy by a supernova explosion that occurred 90 000 years ago. The discovery of this star and two others may help to solve a decades-old debate on how supernovae occur.

Type Ia supernovae are the thermonuclear explosions of white dwarfs in binary star systems. They are the most common type of supernovae and have fundamental importance as cosmological distance indicators. Despite this, the nature of the binary system and the details of the explosion have remained mysteries. Many theoretical models have arisen over the past few decades to explain how these stars explode, but there have been few pieces of direct evidence that any of these scenarios actually succeeds in nature.

One model, dubbed the "dynamically driven double-degenerate double-detonation" (D6) scenario, predicts the possibility that the other star in the binary system is another white dwarf that can survive the explosion of its companion. Such a surviving star would be flung away from the system when the gravitational pull of its companion disappeared and would continue zipping away at speeds between 1000 – 2500 km/s.

Shen et al. (2018) searched for such hypervelocity survivors in Gaia's second data release in April 2018 and discovered three likely candidates. These stars were followed up with ground-based telescopes, including the Southern African Large Telescope (SALT), and found to possess many of the predicted features for survivors of D6 Type Ia supernovae: a lack of hydrogen and strong signatures of carbon, oxygen, and magnesium, as well as luminosities and temperatures unlike almost all other stars. Furthermore, the past location of one of the stars is spatially coincident with a known supernova remnant, making it highly probable that it was ejected from a system that underwent a supernova.
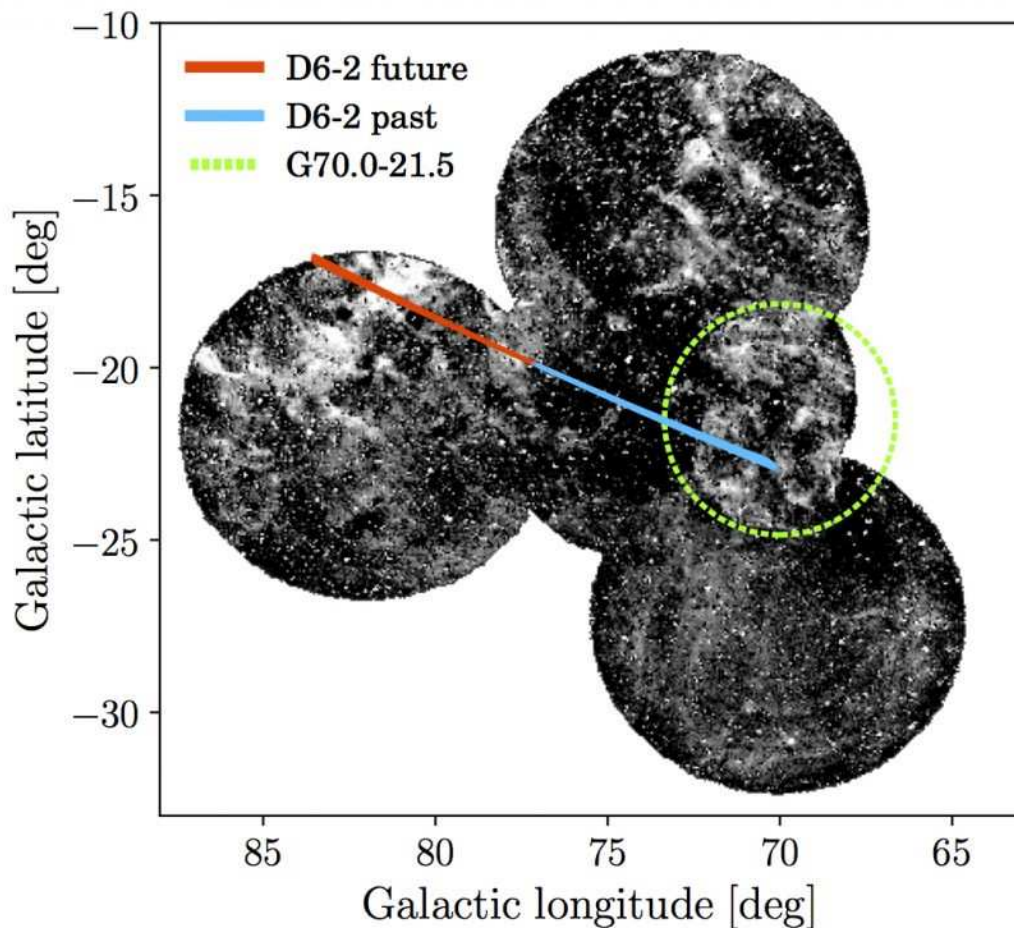
Fig. 1 *Orbital solution of the second white dwarf candidate for the D6-scenario, overlaid with H-alpha images from the Virginia Tech Spectral Line Survey (VTSS, Dennison et al. 1998). The blue trajectory extends 90,000 years into the past, the red trajectory extends the same amount of 90,000 years into the future. The green circle indicates the remnant of the supernova G70.0-21.5. Image credit: Shen et al. (2018)*

The combination of Gaia, which precisely measured the high-speed motion of these hypervelocity stars in the plane of the sky, and the ground-based spectroscopic observations, which provided a measurement of the radial component of the stars' motion, has shown that these are among the fastest freely moving stars in our Milky Way Galaxy.

Much follow-up work remains to be done to ascertain precise characteristics of these stars and the explosions that gave birth to their hypervelocity natures. However, it is very likely that these stars represent the first discoveries of surviving companions to Type Ia supernovae, and that they confirm the success of the D6 "dynamically driven double-degenerate double-detonation" model.
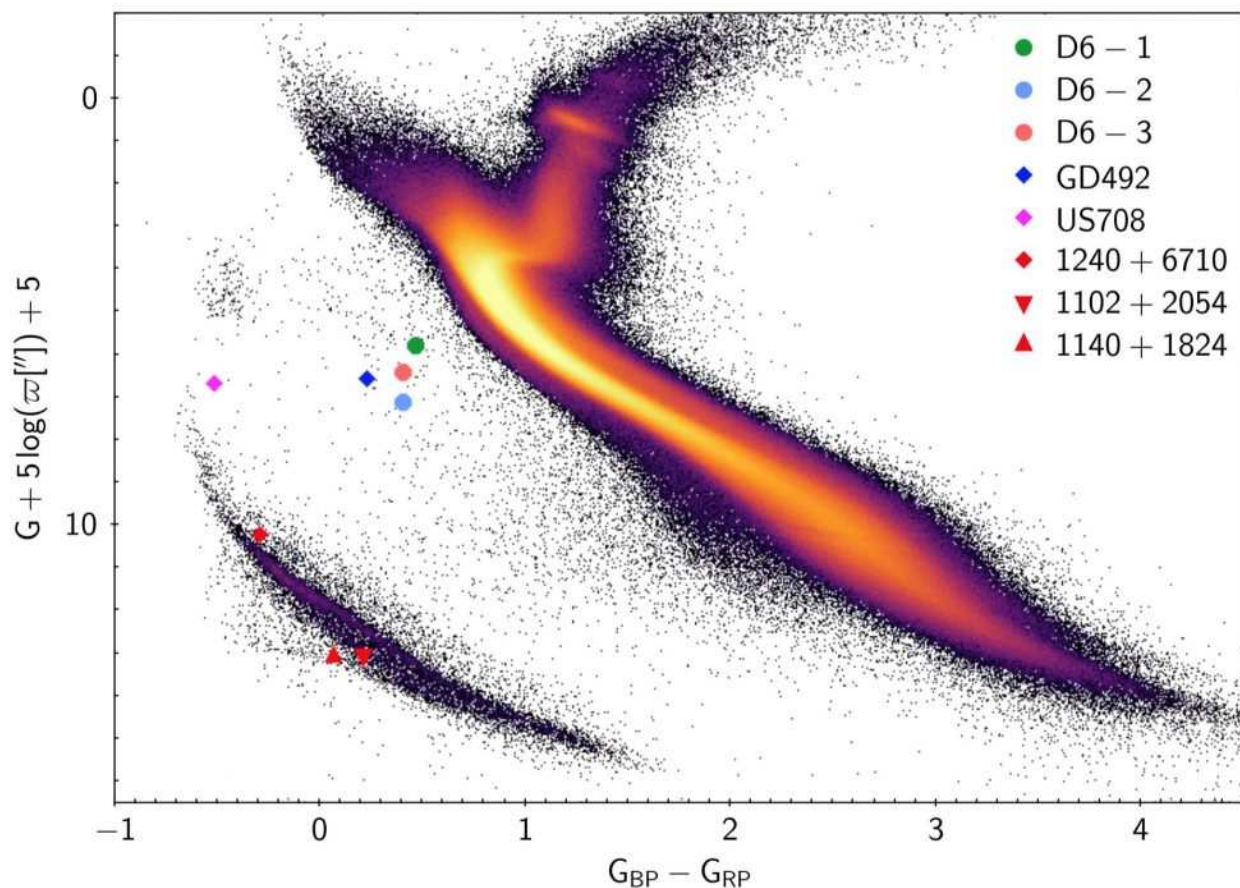
Fig. 2 *The three hypervelocity candidates are shown here in the colour-magnitude diagram with the green, blue and orange circles. Some other white dwarfs are indicated in this diagram as well. The black circles and coloured regions show the reliably measured stars from Gaia. Image credit: Shen et al. (2018)*

The team undertaking the observations and data analysis was led by Ken Shen, a researcher at the University of California at Berkeley (USA). The SALT observations were taken by Marissa Kotze at the Southern African Astronomical Observatory as part of a program led by Saurabh Jha from Rutgers, the State University of New Jersey (USA).

Credit: ApJ, SAAO, Dr Daniel Cunnama and Dr Ken Shen

News Note: SALT plays key role in the global hunt for Dark Energy

The Southern African Large Telescope (SALT), the largest optical telescopes in the Southern Hemisphere, has played an important role as part of the international Dark Energy Survey's, DES, [1] quest to pin down dark energy, the mysterious force accelerating the expansion of the universe.

As part of the hunt, SALT conducted follow-up spectroscopy of supernovae – stars that explode at the end of their lives – discovered by DES. Supernovae are so bright that they can be seen on the other side of the Universe and astronomers can accurately calculate the distances to a small subclass of them – the so-called Type Ia supernovae. Once their distances are known, Type Ia supernovae can be used to measure the acceleration of the expansion of the universe. Sorting through the chaff of variable objects to find and classify the Type Ia jewels was the important role undertaken by SALT and several other of the world's biggest telescopes.

Fig. 1 An example image depicting one of the supernovae that SALT took spectra of. Left: Image of a galaxy before the supernova, Right: Image of the same galaxy after the supernova, with the explosion clearly visible in the left of the galaxy. Credit: SALT/SAAO

Fig. 2 Zoomed in and rotated image of the supernova in Figure 1, highlighting it in one of the host galaxy's spiral arms. For a brief time the supernova can be as bright as the 100 billion stars of the host galaxy. Image Credit: SALT/SAAO

"To measure the acceleration of the universe's expansion by studying stars that died hundreds of millions of years ago takes the most powerful telescopes in the world, combined with meticulous analysis. SALT has provided a key contribution to the international Dark Energy Survey, the most sophisticated study of dark energy

with supernovae yet" said Dr. Eli Kasai, former PhD student at SAAO, now lecturer at the University of Namibia, and Principal Investigator for the South African Astronomical Observatory DES program from 2014 to the end of the survey in 2018.

"We need to control systematic uncertainties to very high precision so that we have confidence in our conclusions. SALT, with its massive mirror and ability to rapidly target exciting new candidates, allows us to take a confirming spectrum when the supernova candidate is at its brightest. This translates into clean answers to exactly what kind of exploding star we are looking at.", said Dr. Mathew Smith, who is based at Southampton University and was the PI of the SALT spectroscopic follow-up program of DES supernova candidates from 2013 to 2014.
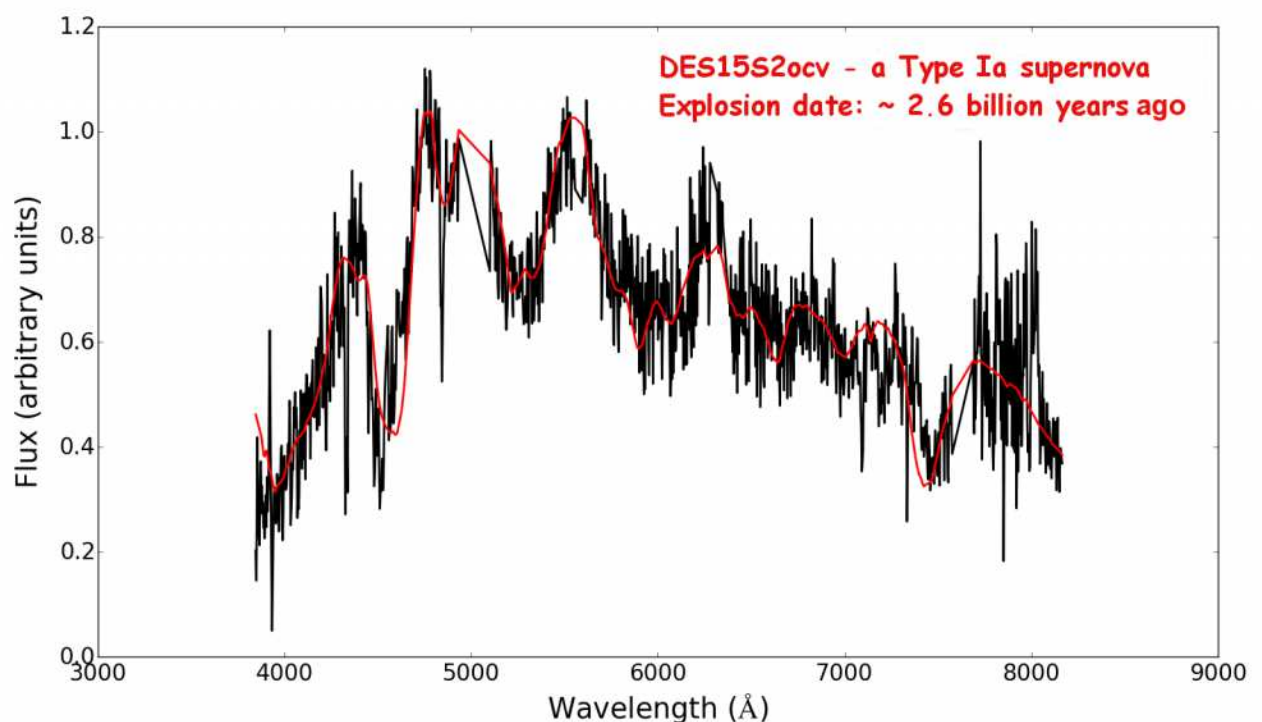
Fig. 3 A spectrum of the Type Ia supernova "DES15S2ocv" taken by SALT on the 9th of January 2016. Over-plotted in red is a template spectrum used to classify the supernova. Image Credit: SALT/SAAO

DES began science observations in 2013, in Chile, South America, with an overall goal of measuring the expansion history of the Universe in order to place tight constraints on the quantity and properties of dark energy at an accuracy of about 1%. DES employs several methods of constraining dark energy, of which supernova observations are a primary tool.

"20 years ago we discovered Dark Energy and the acceleration of the universe by carefully observing supernovae. Today, two decades later, dark energy is still one of the great mysteries of our time. These results, with the purest sample of supernovae to date, confirm yet again that dark energy is real, and will be a key target of

investigation for the Square Kilometre Array (SKA), that will be built primarily in South Africa." said Professor Bruce Bassett, a member of the SALT DES supernova follow-up program, astronomer at SAAO and head of the Data Science group at the South African Radio Astronomical Observatory (SARAO). SARAO has recently completed construction of the MeerKAT radio telescope that will form an important part of the Square Kilometre Array.

"Dark Energy is perceived to exist in the vast empty spaces between galaxies in the Universe known as voids and we believe that it is responsible for making galaxies move away from each other at ever-increasing speeds. In other words, it is responsible for the accelerated expansion of the Universe that we observe" said Prof. Roy Maartens, an SKA Chair in Astrophysics and Cosmology at the University of the Western Cape and a member of the SALT DES supernova follow-up program. He went on saying "observing more and more supernovae in many galaxies gives us a handle to quantify the properties of dark energy and also provides us insight into the true nature of supernovae".

SALT consistently played a pivotal role of classifying into various types the discovered supernova candidates and successfully determining how far they were from Earth, two important parameters that were key to the success of the DES experiment, which came to an end at the end of February 2018. Spectral observations of the discovered SN candidates by SALT and other spectroscopic capable telescopes in DES played a crucial role in helping algorithms that could classify the discovered supernova candidates and determine their redshift using only the images in which such candidates were discovered. This type of classification and redshift determination is less accurate in comparison to that performed with spectroscopic data from SALT and other spectroscopic capable telescopes.

"The DES team has independently confirmed the existence of dark energy by combining four different cosmic probes:

1. supernova observations,
2. baryonic acoustic oscillations,
3. weak gravitational lensing, and
4. galaxy clustering",

said Dr Eli Kasai. He continued by saying "The conclusions from DES from combining these four probes mean that for the first time we have been able to find strong evidence for cosmic acceleration and dark energy from a single experiment, instead of combining results from many different telescopes and different analyses."

The past three weeks have seen the release of 8 DES papers to Arxiv.org, reporting the findings of the analyses of DES supernova data observed over the first three years of the survey. The papers made use of the survey's spectroscopic data including that taken with SALT.[2]

References
1   https://www.darkenergysurvey.org/)
2   https://arxiv.org/search/astroph?query=Bassett+kasai&searchtype=author&abstracts=show&order=-announced_date_first&size=50

Credit: Dr. Eli Kasai: Dr Daniel Cunnama: and Prof. Bruce Basset

News Note: The South African Radio Astronomy Observatory (SARAO) joins the Ceph Foundation to Advance Open Source Storage

More than 30 members have joined the new Ceph Foundation to manage the massive growth in data and information generated from cloud, container and Artificial Intelligence applications

Yesterday in Berlin SARAO joined 30 other members in the establishment of the Ceph Foundation, to manage the massive growth in data and information generated from cloud, container and Artificial Intelligence applications.

The Linux Foundation, a non-profit organization enabling mass innovation through open source, announced that over 30 global technology leaders are forming a new foundation to support the Ceph open source project community. The Ceph project develops a unified distributed storage system providing applications with object, block, and file system interfaces.

"Ceph has a long track record of success when it comes to helping organisations

effectively manage high growth and expanding data storage demands," said Jim Zemlin, Executive Director of the Linux Foundation. "This partnership will assist us to store and retrieve the huge volumes of data that will be collected by the MeerKAT radio telescope," says Dr Rob Adam, Managing Director of SARAO.

Fig 1. Typical MeerKAT antenna.

The MeerKAT is a 64-antenna array radio telescope that has been built on the SKA site in the Karoo, and which will be integrated into the first phase of the Square Kilometre Array. MeerKAT has the capacity to process 275 Gigabytes per second in real time - that equates to approximately 58 DVDs per second. SARAO currently uses Ceph to synthesise a ~20 PB object-based storage system, for the data generated by the MeerKAT radio telescope array.

Ceph is used by cloud providers and enterprises around the world, including financial institutions (Bloomberg, Fidelity), cloud service providers (Rackspace, Linode), academic and government institutions (Massachusetts Open Cloud), telecommunications infrastructure providers (Deutsche Telekom), auto manufacturers (BMW), software solution providers (SAP, Salesforce), and many more.

Ceph is also used by Rook, a Cloud Native Computing Foundation project that brings seamless provisioning of file, block and object storage services into the Kubernetes environment, running the Ceph storage infrastructure in containers alongside applications that are consuming that storage.

Efficient, agile, and massively scalable, Ceph significantly lowers the cost of storing enterprise information in the private cloud and provides high availability to any object, file, and block data. Block and file storage are critical to any IT infrastructure organisation and are important components of infrastructure platforms like OpenStack and Kubernetes.

The growth of new cloud, container and artificial intelligence/machine learning applications are driving the increased use of Ceph. Ceph combined with analytics and machine learning can, for example, enable enterprises to comb through mass amounts of unstructured data to quickly spot patterns in customer behaviour, online customer conversations, and potential noncompliance scenarios.

"A guiding vision for Ceph is to be the state of the art for reliable, scale-out storage, and to do so with 100% open source," said Sage Weil, Ceph co-creator, project leader, and chief architect at Red Hat for Ceph. "While early public cloud providers popularised self-service storage infrastructure, Ceph brings the same set of capabilities to service providers, enterprises, and individuals alike, with the power of a robust development and user community to drive future innovation in the storage space. Today's launch of the Ceph Foundation is a testament to the strength of a diverse open source community coming together to address the explosive growth in data storage and services."

"Ceph was designed and built for scalability, initially with supercomputers and later with cloud infrastructure in mind. A key design premise was that the storage system

needs to provide a highly reliable and available service in a dynamic and increasingly heterogeneous hardware environment where everything can potentially fail," said Carlos Maltzahn of University of California, Santa Cruz, a co-founder of the research project that first created Ceph over a decade ago.

Thomas Bennett, Senior Software Systems Engineer at SARAO says: "SARAO uses Ceph in concert with locally manufactured hardware to lower storage capital expenditure for the MeerKAT storage infrastructure. In order to share our experiences and showcase Ceph, the SARAO storage team is in the process of establishing a Cape Town Ceph community forum." The inaugural meeting for this community forum will take place on the 28 November at the V&A Waterfront in Cape Town.

Associate members include Boston University Information Services and Technology, CERN (European Organization for Nuclear Research), FAS Research Computing - Harvard, Greek Research and Technology Network (GRNET), Monash University, South African Radio Astronomy Observatory (SARAO), Science and Technology Facilities Council (STFC) at UK Research and Innovation (UKRI), and University of California Santa Cruz's Centre for Research in Open Source Software (CROSS).

About the Ceph Foundation
The Ceph Foundation is a directed fund under the Linux Foundation. It provides a neutral home for the Ceph community to collaborate and grow, and is supported by members across multiple industries. Ceph is a unified distributed storage system providing applications object, block, and file system interfaces in a single unified storage cluster—making Ceph flexible, reliable and easy for you to manage. Ceph is built on the Reliable Autonomic Distributed Object Store (RADOS), which provides a highly available and scalable fabric that can either be consumed directly or via higher-level object, block and file services that are built on top.

Bringing history to life – Mars imaging with the 13-inch Boyden Refractor

Clyde Foster

Abstract: The 13" Refractor at Boyden Observatory, Bloemfontein, has a very special Mars heritage, as it was used by Astronomer William Pickering to capture the first ever photographic images of the red planet in 1888. Due to my specific interest in high resolution imaging of Mars, since discovering this heritage, it has always been an ambition of mine to undertake an imaging run of Mars using this telescope. Although it was my original intent, I was unable to visit Bloemfontein close to Mars opposition

in July this year due to an accident earlier in the year which prevented me travelling. However, an opportunity arose in early December, with the University of the Free State(UFS)/Boyden Observatory working closely with ASSA Bloemfontein, myself and the Telescope Shop(Neil and Jess) to co-ordinate an event that incorporated a private showing at Naval Hill planetarium, astro-imaging presentations at Boyden Observatory, a tour of the Observatory and an imaging/observing session on the historic 13" Boyden Refractor as well as other telescopes that had been brought down from Johannesburg by the Telescope shop.

13" Boyden Refractor

The telescope has a primary objective lens of 13" (330 mm), with a focal length of 4 880 mm, corresponding to a focal ratio of 14.8. It was manufactured by Alvan Clark and Sons in Massachusetts, USA in 1887. It was installed at Cambridge and, as noted, was used by William Pickering in May of 1888 to photographically image Mars. Some of the original glass plates of these images are in the possession of UFS.

The telescope then spent some time at Mount Wilson Observatory before being relocated to Peru and installed at the Arequipa station of Harvard Observatory in October 1890. Here it was used for further planetary work as well as double star research.

The optics of the telescope have a fascinating, and possibly unique, characteristic. In one configuration, the primary lens is optimised for visual observing and in the second configuration it is optimised for photographic work.

In the late 1920's the equipment from Arequipa, including the 13" refractor, together with some new equipment, was transported to Bloemfontein, South Africa where the Boyden Observatory was set up, and commenced operation in 1933. In the years since, the Observatory has experienced many highs and lows, but it is good to see that it stands as a living monument to those that have cared for it over the years. Those who are currently responsible are doing a wonderful job of maintaining and restoring the heritage of this gem of South African astronomical history. A wall exhibit which presents the history of the telescope has recently been opened.

Mars Imaging session

The original intent was to arrive on the Friday and run a private imaging session on the 13". Unfortunately this was prevented by an intense storm. With further intense storms being experienced during the Saturday afternoon, there were serious concerns that the imaging and observing sessions would have to be cancelled. However, as the presentations and tour progressed, the skies began to clear and by

the time the sky was darkening, the clouds were gone. Some pre-testing had already been done to ensure that the imaging train would fit onto the refractor and that the necessary software on the laptop was functioning correctly. In many instances, best seeing conditions are experienced in twilight and we were fortunate to be given this imaging slot, which allowed the capture of Mars at its highest elevation.

Fig. 1 Mars 2 December 2018 Boyden Refractor Image set 1756UT RGB IR jpeg

The imaging train:

- Xagyl motorised filter wheel with Baader RGB narrowband, IR/UV cut filterset. The 1 1/4" standard nosepiece of the filterwheel fitted snuggly into the eyepiece holder. An IR>685nm broadband filter was also used.
- ZWO ASI290MM camera. This is monochrome "webcam" and is well recognised in the planetary imaging community as one of the best available at present. It utilises the Sony IMX290LQP uncooled sensor, which is a 1/2.8" CMOS (9mm × 9mm) chip. Pixel size is 2.9micron.
- Assessing the characteristics of the telescope and camera, I had already decided that given the focal length of the telescope I would image at native FR, without any Barlow lens. This would give an image scale of 0.12"/pixel which is favourable compared with the theoretical resolution of the telescope of 0.35".

Software:
- The motorised filter wheel comes with standard software which was installed on the laptop.
- Firecapture v2.6 software (Torsten Edelmann) was used to control the camera.

Data capture:
- The session commenced at 1739UT (1939 local time) and ended at 1814UT (2014 local time), covering a period of 35 minutes.
- My "standard" Mars capture process was followed.
- Multiple 45s SER videos of R, G, B and IR channels were recorded totalling approximately 18GB of data. 3xIR, 6xR, 4xG and 3xB sets of data were captured.

- Capture rate was between 100 and 140FPS with the chip cropped to 640x352 pixels.
- Assistance was provided by Prof Matie Hoffman and Frans Human who managed the RA/Dec adjustments, Shaun Staats, Piet le Roux and Angelique Heyneke.
- The greatest challenge was achieving an accurate focus point which had to me done manually, which is not recommended for this type of imaging.

Data processing
- Pre-processing using PIPP
- Alignment and stacking was done with Autostakkert3!
- Wavelets processing in Registax 6
- De-rotation and colour combine in Winjupos
- Post processing in Photoshop CC

Fig. 2 Observing support team; from l to R – Prof Matie Hofmann, Author, Frans Human, Angelique Heyneke, Shaun Staats

Conclusion:

Although Mars was imaged well past opposition, and at a greatly reduced size of 9", reasonable and acceptable results were obtained. Particularly good data was obtained at green wavelengths. The NASA Curiosity rover and Insight lander sites are

in view. I look forward to the opportunity of future opportunities, possibly at next Mars opposition in 2020.

For the author, who looks forward to the opportunity of possibly doing it again at the next Mars opposition in 2020, the tremendous experience and privilege of executing a Mars imaging run on this historic telescope with its wonderful heritage was a huge personal highlight. The excitement was shared by those present, which added to the occasion.

Acknowledgements
Thanks to the UFS/Boyden Observatory and ASSA Bloemfontein for providing this opportunity; in particular thanks to Prof Matie Hoffman, Dawid van Jaarsveld and Stephan Cilliers, without which it would not have happened. And special thanks to the imaging support team as listed above.

Recent Southern African Fireball Observations

Tim Cooper, Bredell Observatory

Abstract: This article continues the sequential numbering of reported fireball sightings from southern Africa. By definition, a fireball is any meteor event with brightness equal to or greater than visual magnitude (m_v) − 4. The following events were reported to the author and details are reproduced as given by the observer [any comments by the author are given in brackets]. All times were converted to UT unless stated, and all coordinates are for epoch J2000.0.

Event 308 – 2018 June 7 – Redhouse, Port Elizabeth
Observed by Sue Crear at around 04h25, duration about 5 seconds, she commented 'bright yellow streak across the sky, came from a westerly direction, going north horizontally before it just disappeared. Broke up into several pieces like a shower of sparks. It took my breath away'. No further details could be obtained.

Event 309 – 2018 July 14 – Musina, Limpopo
Observed by Conrad de Kock at around 20h00. He and others were sitting around the campfire facing north and saw a bright light mowing from right to left, east to west. He commented 'the whole camp lit up as if it was daylight for a split second, and when we looked to the sky it was as if there was a shooting star very close by'.

Event 310 – 2018 July 25 – Various locations, Gauteng

Observed by Rarda van Oosten at 19h02 from Randburg. Duration 3 seconds, very bright like the Moon, which was near full at the time and magnitude -12. Colour very bright white ball with orange tail that 'seemed to be leaving sparks'. No sounds heard. From sketches provided by Rarda I determined the start and end points as roughly az/alt 313°, 30° to 290°, 10°, where the fireball disappeared below nearby buildings. The path is from very close to Arcturus moving down right to left towards the tail of Leo. The event was also mentioned on social media as being seen by Lorinda Janse van Rensburg from north west of Pretoria, Henning van der Merwe from Brits and Tharina Naude from Fochville.

Event 311 – 2018 July 27 – Vredehoek, Western Cape
Observed by Sarah Chippendale during bright twilight at around 17h30, while walking in Vredehoek, at the intersection of Deerpark Drive West, looking up M H Goldschmidt. The fireball was 10-15° above the horizon, first seen in azimuth 45° and disappeared behind the slope of Devil's Peak in azimuth 98°. Appeared as a blue ball with a white tail, larger than an aircraft and moving more quickly, duration of the 53° path was 3 seconds.

Event 312 – 2018 September 3 – Kloof, KwaZulu Natal
Observed by Yvette Ferreira at around 15h55 from the grounds of Thomas Moore School. She was sitting in her car waiting for her daughter, facing north, the sky was still blue when she saw a very bright orange fireball moving left to right and downwards at an angle of about 45°. From a sketch she provided I calculate the start and end azimuths as 352° to 010°. 'Looked like burning debris falling from the sky, and left a cloud of smoke hanging in the air'. Duration was a few seconds. No sounds heard.

Event 313 – 2018 October 6 – Western and Northern Cape
Tristan Gardner, an airline pilot was routed to Cape Town at 10973m and 60 nautical miles (111km) north east of Sutherland VOR when he saw the fireball at 18h56. They were heading in 227°, the fireball first appeared at around azimuth 137° and appeared to be converging with the aircrafts path. Comet-like appearance [head and tail], colour was said to be bright purple like that seen in arc welding. Fast moving, duration 2-4 seconds and then pulsed and exploded with a bright green flash which momentarily filled the view through the cockpit windscreen.

Also observed by Estie and Charles Clarys from Vanrhynsdorp. Sitting looking due south, Estie produced a sketch showing the fireball moving at a shallow angle low above the horizon from left to right, from azimuth 130° to 210°. Appearance was of a red and white ball with a tail, which burned out without any terminal burst.

Pieter Labuschagne reported on the Sterre en Planete Facebook page, witnessed from 20 km west of Inverdoorn, Bokkeveld, looking south, moving east to west about azimuth/altitude 170°, 40° and downwards to the right towards the horizon which was obscured by mountains up to about 15°. The light was still visible after it dipped below the mountain. Colour was bright blue-green, like a 'mercury security lamp'. Duration was 3-4 seconds, and left a broad glowing trail visible for 5 seconds. The fireball flashed several times, mainly in the second half of its duration and appeared to disintegrate into several pieces which continued to move parallel to each other.

Also reported seen by Lizette Coetzee from Robertson, who said it first looked like lightning before seeing the long streak across the sky, and by Elma Van Coller Viljoen from Franschhoek.

Event 314 – 2018 November 13 – Brackenfell, Western Cape
Observed by Gerda Jacobs at 20h20-20h25, duration about 3 seconds, she said intense bright white/blue, rounded in front, narrower at the back tapering into a white trail and seemed quite close. She was sitting outside facing east in her garden, when the fireball appeared just above her rooftop at azimuth 109°, descending at a shallow angle before disappearing below the roof line at about azimuth 145°. The probable path was from Canis Major, below the bright star Canopus, disappearing from view in Carina and the path is consistent with a bright Taurid fireball. The waxing crescent moon, 33% illuminated, magnitude -10 was in the west and was veiled in thin fog. She said the fireball was brighter than the brightest stars visible (Sirius and Canopus), and possibly as bright as the Moon. Gerda said 'I have never seen a "shooting star" so bright, large and one that seems to be that close. It was really special'.

Acknowledgements
Thanks to Dr Daniel Cunnama (SAAO) and Kos Coronaios (ASSA Observing Director) for forwarding various reports from the public.

Observations of the darkness and colour of the 2018 July 27 Total Lunar Eclipse

Tim Cooper[1] and Percy Jacobs[2]

[1] Bredell Observatory, [2] ASSA Pretoria Centre.

Observation of lunar eclipses by ASSA dates back to the early 1970s. Observations of the total lunar eclipse of 6 August 1971 included nine photographs by N B Dumas (Wild 1971), as well as occultation timings of stars by the eclipsed moon (Muller

1971). These observations said nothing however about the nature of the umbral shadow, which varies from one eclipse to another. The first measurements of umbral geometry, darkness and colour were made during the total lunar eclipse of 24 March 1978 (Cooper 1978) including darkness measurements for the first time using Danjon's scale, following the excellent article by Sinnott (1975). Since then nearly all lunar eclipses visible from South Africa have been observed to measure the colour and darkness of eclipse, and size and shape of the Earth's umbral shadow. The techniques used were discussed in Cooper (2004) and Cooper and Geyser (2004).

Circumstances for the latest total lunar eclipse (TLE) on 27 July 2018 were very favourable for South Africa, as the Moon passed close to the centre of the Earth's shadow with umbral eclipse magnitude M = 1.61, while the altitude of the Moon at mid eclipse was 63° as seen from Johannesburg. This gave the opportunity to conduct measurements without significant interference from a large atmospheric airmass, which would otherwise affect the observed darkness and colour of the eclipse, akin to the effect seen when the moon is rising or setting. Given this opportunity the authors conducted measurements of darkness and colour on this latest eclipse using a variety of techniques. Plans for future observations are presented.

Reasons for variation in darkness and colour of eclipses

While factors influencing the darkness and colour of lunar eclipses were discussed in Cooper (2004), it is useful to briefly summarise these again here. The sun emits radiation across a broad range of the electromagnetic spectrum. In the vicinity of the Earth this flux has a value of around 1351 W/m^2 (Thekaekara et al 1969), the so-called solar constant. Approximately half of this flux comprises visible wavelengths between 400-700nm resulting in the extra-terrestrial spectrum shown in Figure 1 (Chance 2005). Since the moon is airless, this is also the incident energy at the uneclipsed moon's surface. However, during a lunar eclipse, the earth passes between the sun and moon, and obstructs the sunlight from falling onto the moon's surface. One would expect that during a total eclipse, since the sun is entirely hidden as seen from the moon, the moon should appear entirely dark as seen from earth. In fact this is not the case, and normally though the moon is darkened, it remains visible and coloured. The reason is due to refraction of sunlight by the Earth's atmosphere, and the actual darkness and colour are subject to conditions in the portions of the atmosphere through which the sunlight passes at time of eclipse.
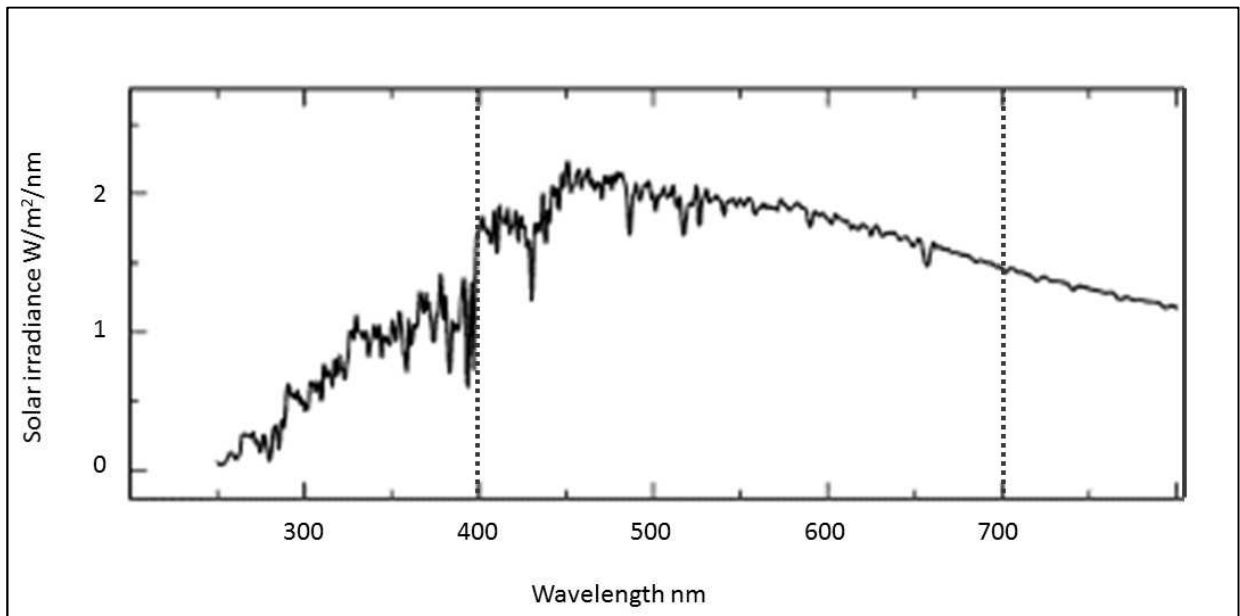
Fig. 1 Low resolution extra-terrestrial solar spectrum (Chance 2005).

Earth's atmosphere comprises five main layers.

- Troposphere, extending to 10-15 km, comprising most of earth's weather. Light is attenuated by clouds, dusts and pollutants
- Stratosphere, extending to around 50 km. This layer contains aerosols from volcanoes, and some pollutants. Light is attenuated by dust particles and molecular gases, and emissions from volcanoes play a significant role.
- Mesosphere, extends to 85 km. Contains some aerosols and meteoric material. In this layer considerable absorption of sunlight takes place by interaction with chemical substances.
- Thermosphere, extends to 600 km, and includes the layers at which most meteoric deflagration occurs.
- Exosphere, outer layers merging with interplanetary space, and comprising mainly hydrogen and helium at very low density.

The first four layers are principally involved in attenuation of sunlight through the processes of refraction, scattering and absorption, but in practice the influence of these processes on lunar eclipses is not significant above an altitude of about 42 km, where the atmospheric density is only around 0.1% that at the Earth's surface (Yapo and Cutler 2009). Therefore conditions in the troposphere and stratosphere are the primary determinants of eclipse colour and darkness. Earth's atmosphere comprises 78% nitrogen, 21% oxygen, less than 1% carbon dioxide and argon, and traces of neon, helium, krypton, xenon, hydrogen, methane and nitrous oxide. Ozone is present in the stratosphere, and nearly all the water vapour is found in the troposphere. Most high energy solar radiation is absorbed in the upper atmosphere

(Friedman 1963) by molecular nitrogen and oxygen between 40-160 km, and by ozone at around 40 km altitude. These absorption bands are known as Hartley Bands. Most infra-red radiation is removed by water vapour in the troposphere. What radiation remains is in the visible region, from about 400 nm to 700 nm. There are several absorption bands in the visible region due to atmospheric gases, and these presumably affect sunlight passing through the atmosphere onto the Moon during an eclipse, depending on the concentration of the absorbing species in the light path at the time. For example, ozone has a broad absorption across the visible spectrum from 450-750 nm (known as Chappuis Bands), but centred around 400 nm. Water vapour absorbs in the region 600-720 nm. Nitrogen dioxide absorbs blue-green light below 600 nm, and photo-dissociates below 400 nm. Nitrate radicals absorb between 410 and 670 nm, and form nitrogen dioxide in the process. If there are significant concentrations of these absorbing species in the light path during eclipse, the transmitted light is deficient in these absorbed wavelengths, resulting in a modification of the colour of light refracted onto the Moon's surface.

At the same time, sunlight is also scattered, due to interaction with small particles. These particles can be dusts originating from particulate pollution due to industrial sources or bio-mass burning, volcanic aerosols or meteoric deflagration products. There are three types of scattering which affect both darkness and colour of the moon:

- Rayleigh scatter – the scattering particles are very small when compared to the wavelengths of sunlight. Light scattering is inversely proportional to the fourth power of the wavelength, and hence blue light is scattered more than red, which preferentially passes through resulting in a redder eclipse.
- Mie scatter – the scattering particles (dust, smoke, and water vapour) are the same size as the wavelengths of light, resulting in blocking of the light and a darker eclipse.
- Non-selective scatter – the scattering particles (water droplets, large dust particles) are much larger than the wavelengths of sunlight, resulting in blocking of sunlight and a darker eclipse.

In addition to absorption and scattering, it has been suggested that eclipse brightness is influenced by solar activity and phosphorescence of lunar rocks. Some terrestrial rocks phosphoresce after irradiation by sunlight, and continue to do so for some time after removal of the exciting radiation. Since the afterglow intensity and time is related to the intensity of exciting radiation, it is supposed that lunar rocks do likewise, and glow brighter and longer around the time of heightened solar activity. This aspect remains to be investigated fully.

The measurement of darkness and colour of lunar eclipses finds applications in researching the terrestrial atmosphere and climate change. For example, Keen (1983) has used ASSA observations as part of his program of monitoring stratospheric aerosols from volcanic origin. He quotes "Since the path length of sunlight through a stratospheric aerosol layer is about 40 times the vertical thickness of the layer, the brightness of the eclipsed moon is extremely sensitive to the amount of aerosols in the stratosphere. Aerosol optical thickness can be calculated from the difference between the observed brightness of the eclipse and a modelled brightness computed for an aerosol-free standard atmosphere, modified by assumed distributions of ozone and cloud". Results of atmospheric optical depth derived from eclipse measurements are shown in Figure 2 (Keen 2018), and indicates the measurement of eclipse darkness is a useful tool to measure the decay of volcanic aerosols. The graph also indicates the atmosphere has been devoid of significant levels of aerosols since the eruption and subsequent decay from Pinatubo in 1991, and the sequence since 1995 has seen relatively bright lunar eclipses.
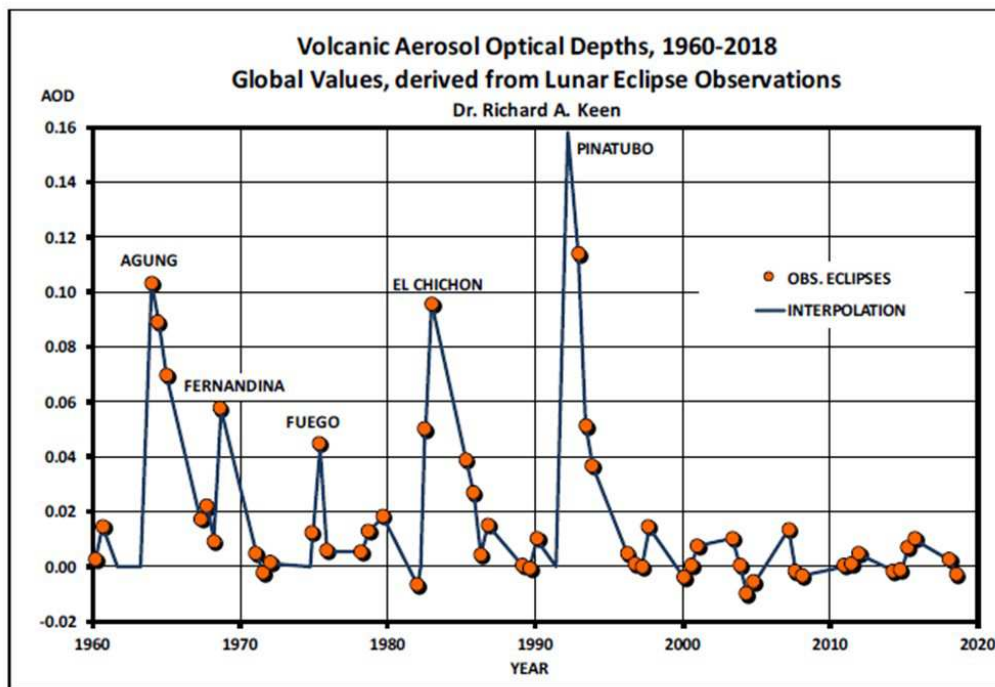

Fig. 2 Volcanic Aerosol Optical Depth (τ_z) determined from eclipse darkness measurements. Major volcanic events are indicated and coincide with very dark eclipses. Diagram courtesy Dr Richard Keen 2018b.

The nett effect then of the three processes of attenuation of sunlight by the Earth's atmosphere during a lunar eclipse (refraction, absorption, and scattering) is to cause the Moon to appear darker and more red than that predicted for a modelled standard atmosphere. These observations form the basis of the ASSA lunar eclipse program.

Circumstances of eclipse

The entire eclipse was visible from South Africa, and the circumstances were very favourable with the moon passing deep inside the umbra, while at a convenient altitude for observation. The full circumstances of eclipse (Espenak 2018) are given in Table 1 (all times are given in UT).

Time (UT)	Event	Altitude of moon at Bredell
17h14m49s	P1 Start of penumbral eclipse	22.2°
18h24m27s	U1 Start of umbral eclipse	37.3°
19h30m15s	U2 Start of total eclipse	51.7°
20h21m44s	Mid eclipse	62.9°
21h13m12s	U3 End of total eclipse	73.8°
22h19m00s	U4 End of umbral eclipse	82.6°
23h28m37s	P4 End of penumbral eclipse	72.1°

Table 1. Circumstances for 2018 July 27 Total Lunar Eclipse

The altitude of the Moon at mid eclipse was 63° as seen from Bredell, corresponding to an airmass of 1.13. Duration of totality was 103 minutes, just 4 minutes shorter than the maximum possible duration, and the umbral magnitude of eclipse at mid totality (M) was 1.61*. This enabled us to determine the darkness and colour with deep immersion within the umbral shadow and without significant attenuation from a large airmass. Given the favourable conditions, we produced the following observations.

*Note magnitude of eclipse (M) here refers to the degree of immersion of the lunar disk into the umbra, and should not be confused with the visual magnitude (m_v) or brightness of the Moon. The value of M is the size of the chord, measured in lunar diameters, which is immersed in the umbra. For a partial eclipse M is between 0 and 1, and for a total eclipse the value of M is >1. Note also that M = 0.5 does not imply that 50% of the moon is obscured, but that 0.5 lunar diameter is immersed in the umbra.

Visual photometry using Selivanov's method

Cooper estimated the brightness of the Moon using Selivanov's reverse binocular method (Sinnott 1975). In this method, the observer diminishes the size of the Moon by viewing it through the objective end of one half of a pair of binoculars. The brightness of the diminished image is then compared with objects of known

brightness, such as bright stars or planets, in the same way as one would estimate the brightness of a variable star using Argelander's method. Keen (1986) showed that the reduced magnitude can be adjusted to give the total magnitude of the eclipsed moon according to the relationship:

$$m_v = RB - (0.2 + (5logM_B)) \qquad (1)$$

where RB is the estimated reversed binocular magnitude and M_B is the magnification of the binoculars. For a pair of 10 x 50 binoculars the correction factor according to (1) would be -5.2 magnitudes, though in practice the value 0.2 may vary slightly depending on the condition of the optics. For this reason the binoculars were calibrated in order to determine a more accurate correction factor, by measuring the reduced brightness of the planets Venus, Jupiter and Mars according to the same comparison star sequence as used for the eclipse brightness measurements. The data obtained is given in Table 2 and confirms the correction for the binoculars used was rather 5.1 magnitudes, so that (1) becomes:

$$m_v = RB - (0.1 + (5logM_B)) \qquad (2)$$

Object	Apparent m_v	Reduced magnitude	Correction
Venus	-3.8	+1.0	4.8
Mars	-2.5	+2.6	5.1
Jupiter	-1.7	+3.4	5.1

Table 2. Calibration values for 10x50 binoculars

Cooper carried out reverse binocular brightness estimates, throughout the eclipse, starting before U1 and ending after U4, and using the comparison sequence in Table 3. These objects were chosen to be in the vicinity of the Moon throughout eclipse, and as a result no corrections for extinction were applied.

Total magnitude m_v was derived from the reduced magnitude estimates using equation (2) and plotted versus time to give a light curve as shown in Figure 3. Times of the key circumstances are indicated on the plot. The total magnitude of the moon at mid-eclipse was determined as $m_v = -1.0$.

Comparison object	m_v		Comparison object	m_v
Venus	-3.8		Mars	-2.5
Jupiter	-1.7		Saturn	0.4
α Aql	0.8		α Sco	1.0
α PsA	1.2		α Gru	1.7
β Gru, σ Sgr	2.0		δ Cap	2.8
β Cap, γ Gru	3.0		α Cap (combined)	3.1
ζ Sgr	3.2		τ Sgr	3.3
θ Cap	4.0		λ Gru	4.4
ν Aqr	4.5			

Table 3 Comparison sequence for RB magnitude estimates
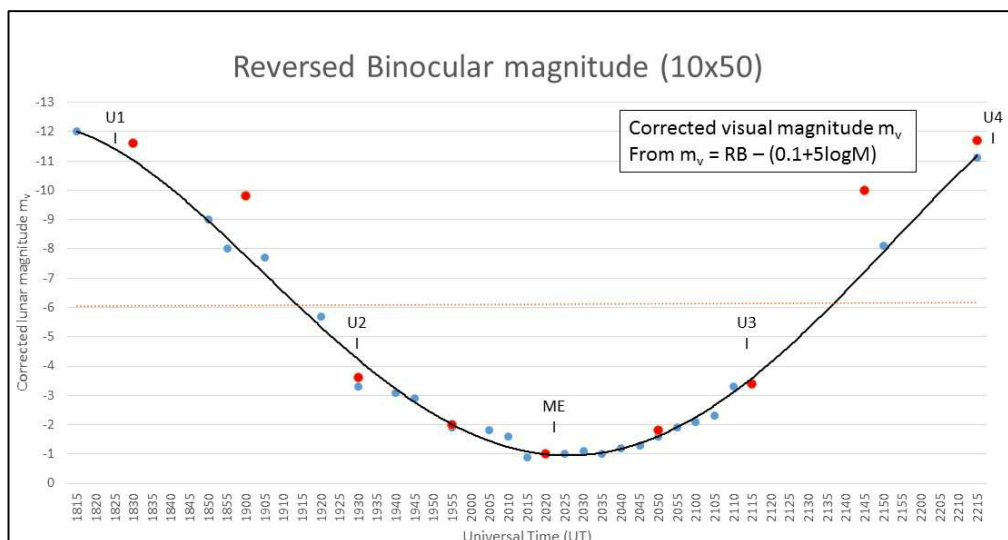
Fig. 3 Light curve of Moon by Cooper derived from reversed binocular brightness estimates (blue dots) and instrumental magnitudes by Di Giovanni derived from lunar eclipse images (red dots).

Keen also carried out reverse binocular brightness estimates using the same sequence in Table 3, though the moon was at lower altitude, from near Rome in Italy. It is useful to compare the brightness from Keen's estimates, where the moon's altitude was only 16° at mid-totality with that of Cooper, where the moon's altitude was 63° at the same instant. As a result of the larger airmass, Keen applied a correction for extinction using the ICQ Tables for magnitude corrections (Green 1992).   The corrected lunar magnitudes are plotted in Figure 4 as solid red dots, while the estimates of Cooper are shown as solid blue triangles. The brightness predicted from Keen's model of the atmosphere free of volcanic aerosols is shown as a black curve, and the brightness determined while the moon was at high altitude is generally in

good agreement. The estimates made at low lunar altitude and which were corrected for extinction show a systematically higher eclipse brightness, and further investigation is required to develop realistic corrections for both reverse binocular and Danjon estimates when the Moon is low in the sky. Nevertheless, Keen's determination of the lunar magnitude at mid eclipse as $m_v = -1.5$ and Cooper's value of -1.0 are indicative of a bright eclipse and a clean atmosphere relatively free of volcanic aerosols.
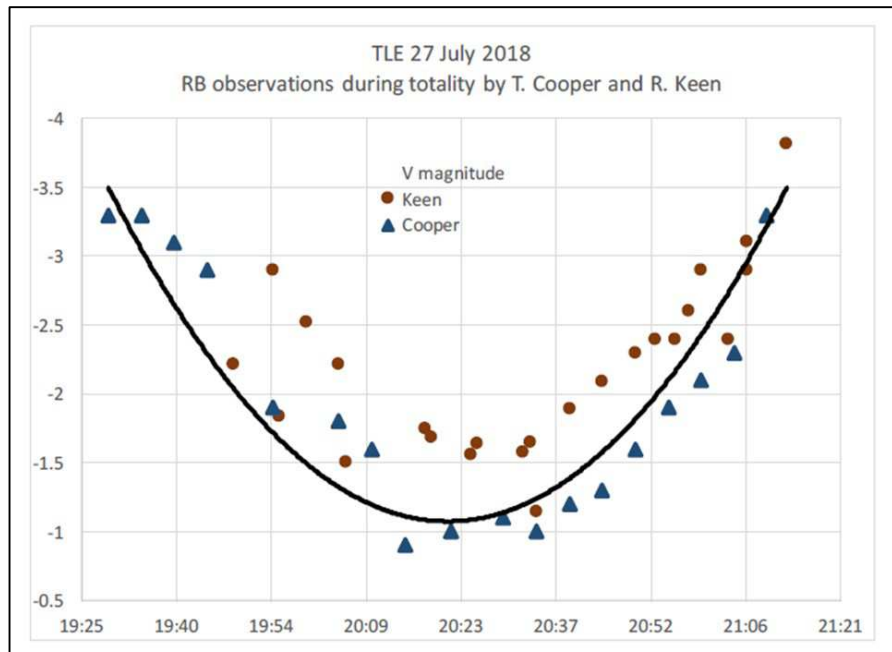
Fig. 4 Brightness of the Moon during totality from reversed binocular estimates by Cooper (solid blue triangles) and Keen (solid red dots). The black curve is the "predicted" brightness during totality using Keen's volcanic-free model. Note the estimates made at low altitude and corrected for extinction result in a brighter eclipse then predicted. Diagram courtesy Dr Richard Keen 2018b.

Lunar photometry using digital images

Di Giovanni (2018) has developed procedures to measure the brightness of the Moon in RGB colour bands using images taken with conventional DSLR cameras. Due to the low altitude of the eclipse from his observing site in Italy, he requested participation of ASSA to obtain images of the Moon located higher in the sky as seen from South Africa. Accordingly Smit and Geyser produced a set of images at various stages of the eclipse according to the schedule supplied by Di Giovanni and given in Table 4. Some examples of the images are shown in Figure 5.
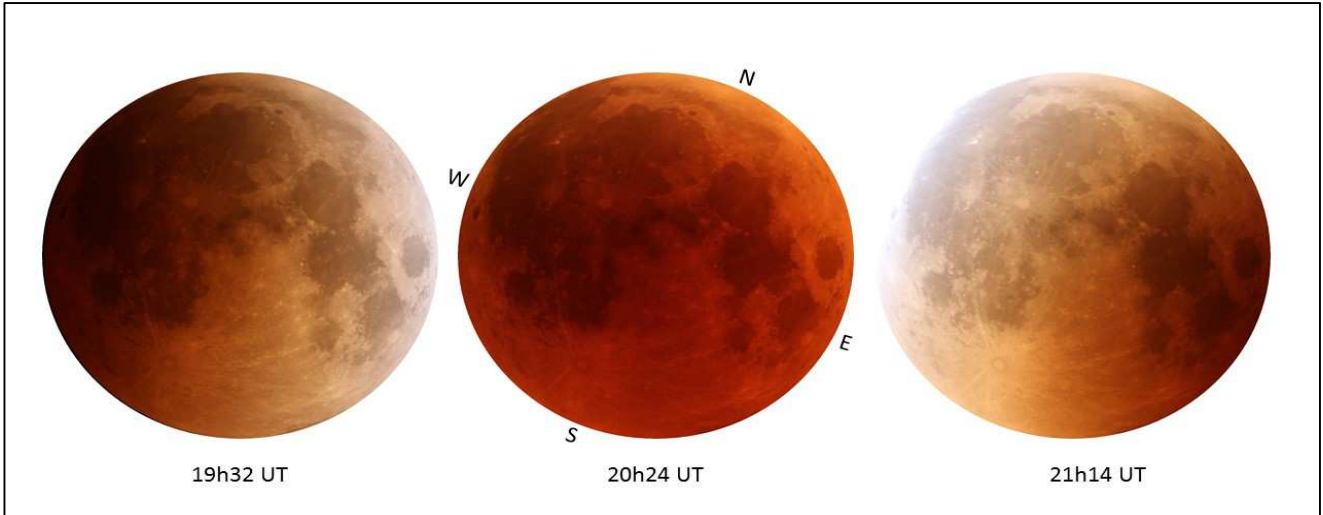
Fig. 5 Examples of images used for determining total lunar magnitude by Di Giovanni. Images by Mauritz Geyser. Note the directions are in the selenographic coordinate system.

Time of image (UT)	Notes
18h30	Initial phase, immediately after U1, showing maximum effect of penumbral shading.
19h00	Moon partially immersed in umbral shadow.
19h30	Beginning of total eclipse, U2, showing brightness in outer extremities of umbral shadow.
19h55	Moon between shadow centre and edge of umbra (point of internal tangency).
20h22	Mid eclipse, moon closest to centre of umbra.
20h50	Moon between shadow centre and edge of umbra (point of internal tangency).
21h13	End of total eclipse, U3, showing brightness in outer extremities of umbral shadow.
21h46	Moon partially immersed in umbral shadow.
22h19	Just before U4, moon tangential to umbral shadow.
22h45	Moon partially immersed in umbral shadow.
After 23h28	Moon out of eclipse, used as reference.

Table 4. Schedule of DSLR imaging for RGB photometry

Using these images Di Giovanni produced brightness contour maps in three bands, and brightness profiles across the moons disk. As examples, those for time of mid eclipse are shown in Figures 6 and 7. By integrating brightness measurements he derived the total magnitude of the moon at each of the scheduled times in Table 4, and the results are shown as red dots in Figure 3. The average lunar magnitude for the whole Moon at mid-eclipse was determined as $m_v = -1.0$, in exact agreement with the value derived from Cooper's reversed binocular estimates. In fact the results determined by both methods show excellent agreement during the periods when the eclipse was in the advanced umbra, and deviate only when the moon was bright. We ascribe these deviations to two possible factors, in the case of the reverse binocular estimates due to a lack of bright comparison objects with which to visually compare the uneclipsed Moon, and due to diffusion of light within the telescope optical tube and in the air resulting in difficulty in reducing pixel counts in the brighter digital images. These problems will receive attention in an attempt to improve future eclipse measurements.
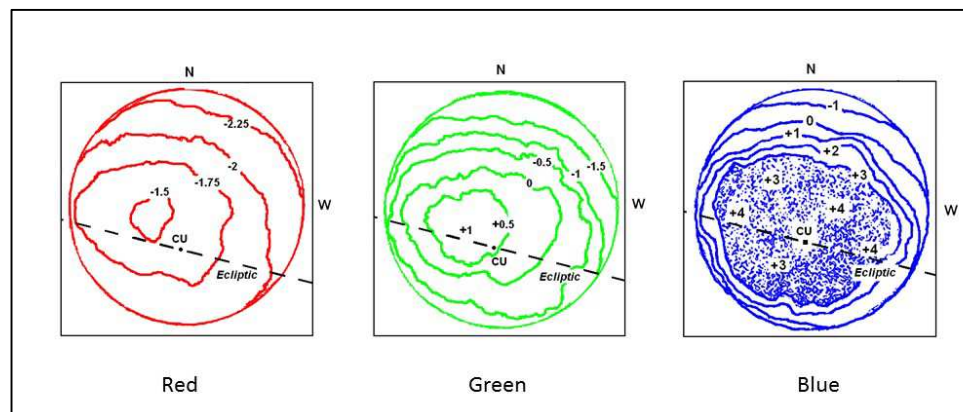

Fig. 6 Isophotal maps for Moon at mid eclipse (20h22UT) in RGB colours. Values of isophotes are visual magnitude mv. Note the directions are in geographic coordinates of the umbra as opposed to selenographic coordinates used in the lunar images. The point marked CU is the geometric centre of the umbra. Diagrams courtesy Giovanni Di Giovanni.
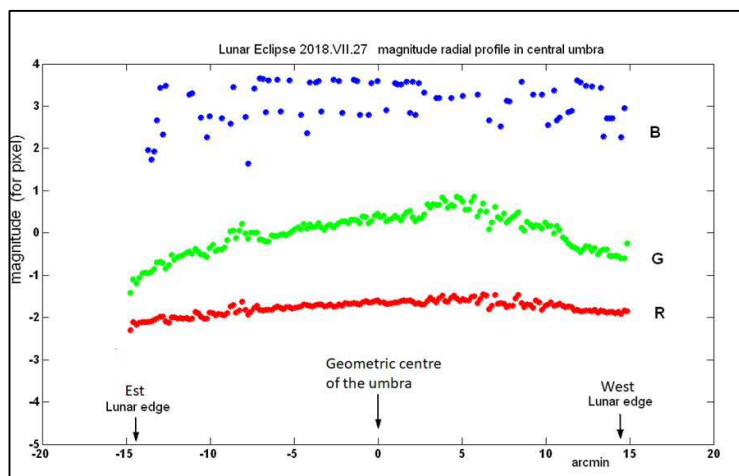

Fig. 7 Instrumental magnitude radial profile across the Moon at mid eclipse in RGB colours, from images by Smit and Geyser. East and West edges are geographic coordinates of the umbra. Diagram courtesy Giovanni Di Giovanni.

Visual photometry using the Danjon method

The French astronomer André Danjon (1920) introduced a five point scale to determine the relative luminosity of lunar eclipses. This scale has proved useful in describing the general colour and darkness of eclipses over a long period, even if the estimate may vary considerably between individual observers, and has been estimated by Cooper for every total lunar eclipse observed since 1978. In the Danjon method, the observer compares the appearance of the eclipsed Moon with the scale, as follows:

L=0   Very dark eclipse, Moon almost invisible, especially in mid totality

L=1   Dark eclipse, grey or brownish colouration; details distinguishable only with difficulty

L=2   Deep red or rust coloured eclipse, with a very dark central part in the umbra and the outer rim of the umbra relatively bright

L=3   Brick red eclipse, usually with a bright or yellow rim to the umbra

L=4   Very bright copper red or orange eclipse, with a bluish, very bright umbral rim.

As can be seen, estimation of the L value can give useful clues to both the darkness and colour of lunar eclipses. A fractional estimate can also be made, so if one feels the description is between L=2 and 3, one reports L=2.5. The estimate is normally made using the naked eye or binoculars and so is well suited to the observer without technical equipment. Keen [1986] has shown there is a good relationship between the L value and the total magnitude of the eclipsed moon according to the formula:

$$m_v = 3.99 - 3.13L + 0.364L^2 \qquad (3)$$

With the foregoing in mind, a call was made on some astronomical social media groups requesting their members to make estimates of L value at mid-totality. The membership of these groups numbers over eight thousand, and seeing as there was widespread interest in this eclipse on these groups it was hoped a large number of members of the public could be persuaded to estimate the L value using their naked eye. The intention was to generate sufficient statistically relevant data as part of a 'citizen science' initiative, and to see how the public perception of the brightness of the eclipse correlated with the methods already described. Alas in the event almost no members of these groups responded, and this aspect of our program was abandoned. Only six estimates of L value were received as listed in Table 5.

Observer	L Value at 20h22 UT
Lafras Smit	3.5
Christopher Cooper	3.5
Tim Cooper	3.2
Stewart Wasserfall	2.5
Carmen Wasserfall	2.0
Nita Planck	1.0

Table 5. Danjon L value estimates for 2018 July 27 eclipse. All estimates were made at mid eclipse to ensure consistency.

The mean value L is 2.62, and inserting into (3) gives a total lunar magnitude at mid eclipse of $m_v = -1.7$. However, the coefficient of variation on these few observations is 38%, which indicates the difficulty in drawing any definite conclusions in the absence of more statistically relevant data. It is disappointing then that so few members of the public were prepared to attempt these simple estimates in order to provide a better correlation to instrumental methods.

Visual and Differential Colourimetry

As explained previously colours seen during a lunar eclipse depend on conditions in the Earth's atmosphere at time of eclipse. In the case of bright eclipses typical colours reported are orange or copper, with yellow and blue at the extremities of the umbral shadow. As the eclipse becomes darker, the observed colour tends towards brick red or rust colour, and for very dark eclipses brown and dark grey are typical. These perceptions are exactly the basis of Danjon's scale, so that observations of L value can also be used to infer the general eclipse colour. For example, Cooper's rating of L=3.2, i.e. slightly on the higher side of 3, was based on his perception of more orange colours than deep reds. However, for any one eclipse the colours seen are also dependant on the observer's perception, and this can be seen in the diversity of L values in Table 5. The mean value of 2.6 is consistent with the description of the moon at mid eclipse as between deep red or rust coloured and brick red, with a dark central umbra and brightish yellow outer rim. This description is no too dissimilar with the visual descriptions made by Cooper during eclipse, except that he observed more orange than red. His descriptions follow, and are also depicted in sketches made in the field, reproduced as Figure 8.

18h42 – partially eclipsed portion already dull copper colour in 16" telescope.
19h30 – start of total eclipse, bright copper orange to naked eye.
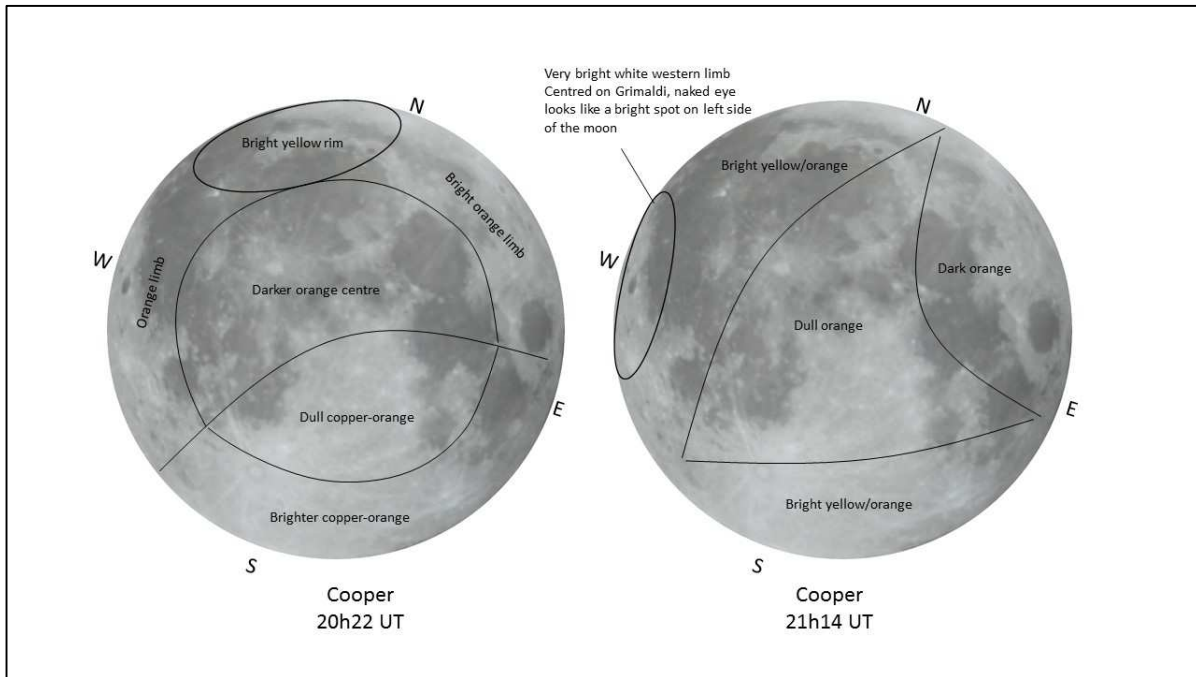
Fig. 8 Visual observations of colour by Cooper. Note the directions are in the selenographic coordinate system.

20h22 – mid-totality, more orange than dark red, L = 3 or even 3.2. Moon has a doughnut appearance to the naked eye with a dark centre surrounded by a brighter ring extending right round the moon. NNW limb bright yellow around Sinus Iridum extending from Aristarchus to Plato, W limb orange and NE limb brighter orange, bright copper orange extending from S to E limb.

20h57 – suddenly very bright white at W limb, centred around Grimaldi.

21h10 – NW limb bright orange, S to E limb bright yellow/orange, with definite white spot on W limb, which appears silvery in 16" telescope 21h14 – central moon dull orange, darker orange towards NE quadrant, with brighter orange NW and SE sectors, and prominent bright white on W side of moon. [The western limb brightening can be seen in the image by Smit taken at 21h14 UT, see Figure 9].
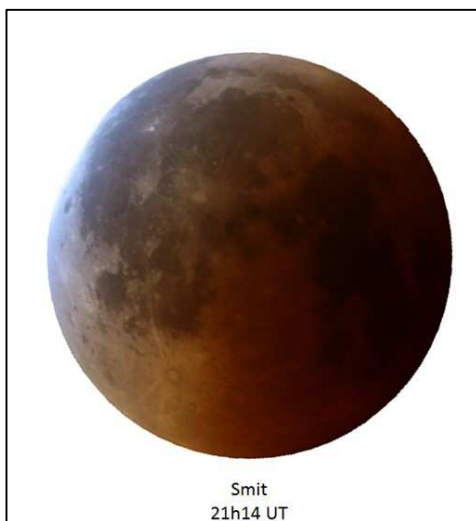
Fig. 9 Image by Lafras Smit taken at 21h14 UT showing brightness at moon's western limb in the vicinity of crater Grimaldi.

To test the reliability of these visual descriptions Cooper determined instrumental colour values on the images produced by Smit and Geyser. Colour of printed images can be visualised in three dimensions using the CIELab tri-stimulus values L*, a* and b*, as shown in Figure 10. These values are based on the Opponent Colour Theory postulated by Hering (1920, 1964) which states that the human visual system interprets information about colour by processing signals from cones and rods in an antagonistic manner. In this theory the human perception of colour can be represented by three pairs of opposite stimuli:

L* – light and dark, where a value of 0 represents darkest black, and 100 represents brightest white.
a* – indicates the colour is red if the value is positive and green if negative.
b* – indicates the colour is yellow if the value is positive and blue if negative.

Fig. 10 CieLab colour coordinates in three dimensional space.
Image credit BYK Corp.
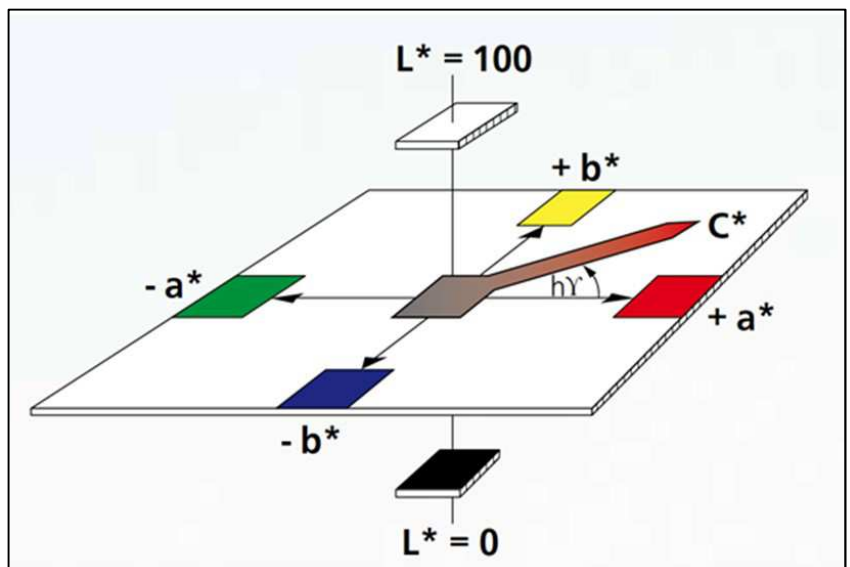
The methodology is described in ISO 11664 Part 4 (2008) which 'specifies the method of calculating the coordinates of the CIE 1976 L*a*b* colour space including correlates of lightness, chroma and hue. It includes two methods for calculating Euclidean distances in this space to represent the perceived magnitude of colour differences'. Looking at Figure 10 one can see that a pure red would have a positive value for a*, and the value of b* would be zero, i.e. no yellow or blue shade. As the value of b* becomes positive, the shade of red becomes increasingly yellow, and the nett perception of colour by the observer is orange. Conversely as the value of b* becomes negative, the shade of red becomes less yellow and more blue. Opposite colours on each axis can never be perceived together, so for example green can never be perceived in the reddened moon.

Images in and out of eclipse were printed on 160 CIE-whiteness plain paper using a Canon MF635Cx colour laser printer. Colour was measured at various positions on the Moon's disk using a BYK Spectro-Guide 45/0 spectrophotometer, using a D65 source and 10° measuring angle, to yield colour coordinates as shown in Table 6. These coordinates are reported as the difference (Δ) between the colour in eclipse

and that of the image after P4 taken at 23h28, that is after the Moon had left the penumbral shadow.

	Selenographic coordinates of measuring point				
	+45°, -15°	0°, 0°	-30°, +50°	-10°, -43°	-55°, -15°
Location	SE quadrant, crater Colombo	Central moon, S of Sinus Medii	N limb, N of Sinus Iridum	S highlands, E of Tycho	W limb. S of Bullialdus
ΔL*	-25.0	-29.7	-10.2	-37.0	-29.3
Δa*	+30.5	+20.5	+13.4	+33.6	+24.6
Δb*	+28.2	+19.4	+38.4	+26.5	+22.0

Table 6. Differential colour measurements, middle image of Figure4 taken at 20h24 UT, just after maximum eclipse. Selenographic coordinates are lunar latitude, longitude.

Colour measurements at all locations within the umbra show strong positive a* values as expected. The mean redness for the five locations was +24.5 which corresponds with the exact colour of the W limb nearby craters Bullialdus and Grimaldi. Furthermore, all locations show strongly positive b* values, the mean value being +26.9, indicating considerable yellow shading of the red colour, so that the overall colour of eclipse is best described as orange. The most red part of the Moon at maximum eclipse was the S Highlands, around the location of the bright crater Tycho. Here b* is also high, so that the colour is more aptly described as orange. The least red and most yellow region is the N limb around Sinus Iridum, a*=13.4, b*=38.4, which confirms with the bright yellow NNW rim observed by Cooper and shown in Figure 8 left.

We also measured the colour at the same points in the image by Smit taken at 21h14 and shown as Figure 9. This image was taken after the appearance of the bright spot at the W limb. Colour measurements here showed that a*/b* values have shifted from 24.6/22.0 to 3.6/0.2, confirming the absence of red or yellow colour in this part of the umbral shadow.

The L* value indicates the light and dark component of the visual tri-stimulus, the lower the value the darker the region. However, since the images were not taken at constant exposure conditions, the L* value cannot be correlated to the photometric measurements reported previously. Rather ΔL* can be used to indicate areas of the umbra that showed greatest change in darkness during eclipse, which is L*= –37.0 in the region of the S highlands. The bright N limb shows least darkening with L*= –10.2.

The overall measurement of a bright red eclipse with strong yellow shading is consistent with a bright orange eclipse and appear to be in good agreement with Cooper's Danjon value of L=3.2.

Spectroscopy

In an attempt to correlate colours seen during eclipse with specific spectral features, Jacobs conducted spectroscopy of the lunar surface in and out of eclipse. He secured images using a Canon 650D camera with Celestron 80mm refractor fitted with a LOWSPEC 600L/mm spectrograph. The spectrograph was positioned so that the slit was oriented across an expanse of lunar maria extending from eastern Oceanus Procellarum through Mare Nubium as shown in Figure 11. This area was selected as being fairly flat terrain to avoid major differences in lunar brightness along the slit. The telescope was mounted equatorially on a Celestron CGEM DX tracking mount and guided with a ZWO ASI 130mm camera. Four spectra were taken as shown in Table 7, but note that the spectrum of the moon before start of eclipse was with the moon at low altitude.

Figure 11 Slit position for spectral images taken by Jacobs.

Time	Exposure	Lunar altitude	Umbral immersion
16h55	4 sec / ISO 100	18°	Before P1
19h50	270 sec / ISO 3200	56°	20 min after U2
20h07	300 sec / ISO 3200	60°	15 min before ME
20h25	300 sec / ISO 3200	63°	3 min after ME

Table 7. Details of spectral images taken by Jacobs

All images were processed with BASS software, including dark and flat calibrations, and corrected for infra-red and atmospheric extinction. The resultant spectra are shown in Figure 12. The spectra for all three exposures taken during totality appear similar, with no major differences in absorption features with depth of immersion in the umbra. Comparing the three spectra during eclipse to the IR-corrected spectrum out of eclipse (pink line in Figure 12, compare also with Figure 1) many features have disappeared, such as the lines for neutral Mg, Ca and Fe, or are considerably

diminished, such as the Hβ and Hα lines, respectively at 486.1 and 656.3 nm, though the latter appears to be broadened. The effect is the same for the Na doublet at 589.0/589.6 nm, which appears diminished and broadened. The Telluric oxygen absorption at 628.0 nm is seen to be more pronounced in the eclipsed spectra compared to the spectrum of the uneclipsed moon. There are two features visible in all three eclipsed spectra, but not in the uneclipsed moon. There is a very broad absorption in the region 570-585nm, and this feature is also seen in spectra of the 8 October 2014 eclipse (Berry 2015) and may be due to atmospheric ozone (Yan et al 2014). Yan states that this band is so strong that it is able to affect the colour of the eclipsed Moon. The absorptions seen around 575 nm and 645 nm may also be due to two of the collision induced absorption (CIA) O_2-O_2 bands from atmospheric molecular oxygen (Yan et al 2014). The degree to which all of these are present in future eclipses will be investigated.

Fig. 12 Spectra acquired by Jacobs. Upper image is the uneclipsed moon at 16h55 UT, lower image is near mid-totality at 20h25 UT. Images have been aligned to the absorption lines in the graphical spectra above. Pink line is the spectrum of the moon out of eclipse, compare also with the low resolution spectrum in Figure 1.
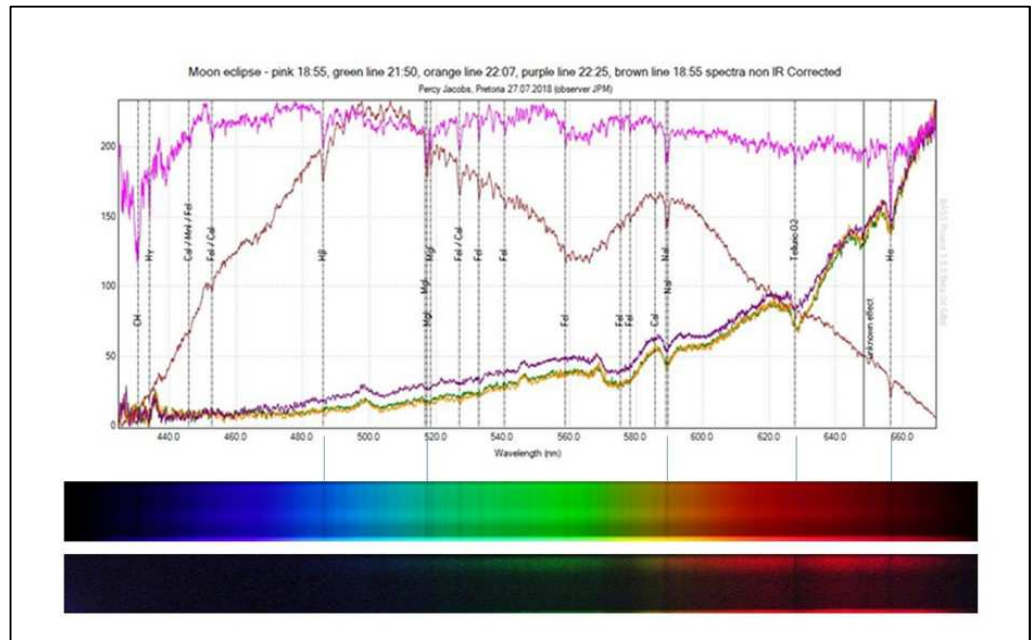
A number of features reported by Berry (2014) are not visible in Jacobs' spectra. The difference could be in that Berry positioned the slit crossing the bright southern highlands intersecting the bright crater Tycho, where the mean lunar albedo is around 0.14-0.17, whereas Jacobs slit lay mainly across the darker maria, where the mean albedo is only 0.05-0.06 (Saari and Shorthill 1971). Berry mentions that the brightness profile across Tycho was visible as a pattern in his spectra, which was our thinking to avoid by placing the slit across the more uniform, but darker maria. In retrospect this may have been the wrong approach [note Cooper was responsible for this decision] and spectral differences between areas of differing albedos may be investigated in future.

Apart from the broad bands due to O_3 and O_2-O_2, there do not seem to be any other major differences that could affect the colour of the eclipsed moon due to absorption. The major difference in and out of eclipse is the broad attenuation at the blue end of the spectrum, which is the result of Rayleigh scatter, and the primary determinant in the red colour of the eclipse. The shape of the spectrum is similar at all three positions in the umbra between first contact and mid-eclipse, and attempts will be made to model this shape further. It is regrettable that we did not secure spectra after mid-eclipse since the position of the slit towards the western side of the moon may have captured some spectral differences with the onset of the whitening at the western limb after around 21h00 UT.

Conclusions and plans for future eclipses

Total visual magnitude of the Moon as determined by visual (reversed binocular) and digital photometry was found to be $m_v = -1.0$ to -1.5, corresponding with an aerosol optical depth τ near zero. This indicates a bright eclipse, and continued very low levels of atmospheric aerosols.

Total visual magnitude determined using Danjon's method gave $m_v = -1.7$, but this was from a very small data set and shows considerable scatter. The call for a large number of estimates on social media met with very poor response. Despite this lost opportunity a call will be made again for public participation for future lunar eclipses, though it will be some time before we experience an event as favourable.

Visual colour estimates by Cooper indicate considerable orange colouration rather than deep red, with a bright, yellow umbral rim. These descriptions are consistent with a brighter eclipse. The visual colour estimates were confirmed by CieLab colour measurement, which in addition to strongly positive a* values, gave positive b* values, indicative of strong yellow shading and a bright orange eclipse. Instrumental colour measurements will be explored further to determine whether these can be correlated with darkness measurements using the Danjon method and to measure colour changes within the umbra throughout eclipse.

Spectroscopy of the Moon out of eclipse showed the expected solar absorption bands due to Hα and Hβ, and the metals Ca, Mg, Na and Fe, as well as Telluric oxygen. In line with passage through a larger airmass the Telluric O_2 line was enhanced and broadened in the eclipsed spectra. The Na doublet was diminished but broadened. The eclipsed spectra show two additional bands not present in the reflectance spectrum out of eclipse, probably due to O_3 and collision induced absorption by O_2-O_2. These were the only absorptions found which may have affected eclipse colour.

The spectra during eclipse show considerable attenuation in the blue region due to absorption by the O_3 Chappuis bands, but mainly due to Rayleigh scatter. Attempts will be made to model the shape of the spectrum to correlate this with colourimetric measurements.

The next total lunar eclipse we intend to observe from South Africa occurs on 2022 May 16, though conditions are not as favourable as morning twilight interferes before mid-eclipse, with the Moon at low altitude, and sets shortly thereafter.

References

Berry, R. (2015), *Spectroscopic Observation of the 2014 October 8 Total Lunar Eclipse*, The Society for Astronomical Sciences 34th Annual Symposium on Telescope Science. Published by Society for Astronomical Sciences, 2015, pp.21-26

Chance, K. (2005) *Ultraviolet and visible spectroscopy and spaceborne remote sensing of the Earth's atmosphere*, C R Physique 6, 836-847.

Cooper, T. P. (1978), *Total eclipse of the Moon 1978 March 24*, MNASSA, Vol. 37, p74.

Cooper, T. P. (2004), *The darkness and colour of the umbra during a lunar eclipse*, MNASSA Vol. 63, pp 60-64.

Cooper, T. P. and Geyser M. (2004), *Size and shape of the umbra during a lunar eclipse*, MNASSA Vol. 63, pp 12-19.

Danjon, A. (1920), *Sur une relation entre l'éclairement de la lune éclipsée et l'activité solaire*, Comp. Rend. 171, p1127, and *Nouvelle détermination de la période solaire basée sur la loi d'éclairement des éclipses de lune*, ibid p1207.

Di Giovanni, G. (2018), *Lunar eclipse brightness and the terrestrial atmosphere*, J. Br. Astron. Assoc. 128, 1,

Espenak, F. (2018), Eclipse Contacts: Total Lunar Eclipse of 2018 Jul 27, downloaded from http://eclipsewise.com/lunar/LEprime/2001-2100/LE2018Jul27Tprime.html.

Friedman, H. (1963) *Ultraviolet and X Rays from the Sun*, Annual Review of Astronomy and Astrophysics, vol. 1, p.59

Green, D. W. E. (1992) *Magnitude corrections for atmospheric extinction*, in International Comet Quarterly, Vol. 14, p55.

Hering, E. (1920, 1964). *Outlines of a Theory of the Light Sense*, Translated from the original German, Hering, Ewald. 1920. *Grundzüge der Lehre vom Lichtsinn*. Berlin: Springer, by L.M. Hurvich and D Jameson. Cambridge, MA: Harvard University Press).

ISO (2008), Colorimetry -- Part 4: CIE 1976 L*a*b* Colour space, in ISO 11664-4:2008. See https://www.iso.org/standard/52497.html.

Keen, R. A. (1983), *Volcanic aerosols and lunar eclipses*, Science, Vol. 222 no. 4627, pp. 1011-1013.

Keen, R. A. (1986), personal communication dated 18 September 1986.

Keen, R. A. (2018a), in *Dull Grey or Copper-Orange: What Will 2018's and 2019's Lunar Eclipses Look Like?*, downloaded from
http://www.eclipsewise.com/lunar/LEnews/LEmore/TLE2018keen.html

Keen, R. A. (2018b), private communications dated 28 November and 11 December 2018

Muller, G. J., (1971), *Occultation of ZC3091 during the Total Eclipse of the Moon on 1971 August 6*, MNASSA Vol. 30, p120.

Saari, J. M. and Shorthill, R. W., (1971), *The Sunlit Lunar Surface*, The Moon Vol. 5, pp161-178, Kluwer Academic Publishers

Sinnott, R. W. (1975), *An Observers Kit for This Month's Lunar Eclipse*, Sky and Telescope, Vol. 49, No.5 (May 1975), pp280-283.

Thekaekara, M, P., Kruger, R. and Duncan, C.H. (1969), *Solar Irradiance Measurements from a Research Aircraft,* Applied Optics Vol. 8, Issue 8, pp. 1713-1732. See also Thekaekara, M. P. (1970) *The solar constant and the solar spectrum measured from a research aircraft*, NASA Technical Report R-351.

Wild, P. A. T., (1971), *Amateurs photographs of August lunar eclipse*, MNASSA Vol. 30, p128.

Yan, F., Fosbury, R. A. E., Petr-Gotzens, M. G., Zhao, G., Wang, W., Wang, L., Liu, Y. and Pallé, E. (2014), *High resolution transmission spectrum of the Earth's atmosphere -- Seeing Earth as an exoplanet using a lunar eclipse*, International Journal of Astrobiology, 14 (2), 255-266 (2015)

Yapo, T. C. and Cutler, B., (2009) *Rendering Lunar Eclipses*, paper prepared for Graphics Interface.

Observing an Exoplanet Transit

Neville Young

Abstract: An experimental test on the ability to observe an extrasolar planetary transit using limited photometric equipment from an Earth based Amateur Observatory

Introduction

In 2017 José da Silva, a colleague at the Pretoria Centre of the ASSA, delivered a presentation on "*Observing transiting exoplanets from your back yard*". In the talk it was suggested that it would be possible observe the dimming effect of an exoplanet

planet transiting its host star using limited equipment. Having recently completed the Soniville Observatory and up-graded the 250 mm SCT, it was time to see if such observations were possible.

José da Silva had successfully observed such transits using the 350 mm telescope in the UNISA Observatory. Lacking the required conditions to repeat his observations, he agreed to repeat the exercise using the smaller telescope in the Soniville Observatory and his expertise; equipment available:

- Telescope: Meade 10", Model 2120 (circa 1988)
- Camera: DSLR, Canon1100D, unmodified
- Configuration: Camera at Prime Focus through a Focal Reducer
- Imaging Software: Backyard EOS, version 3.

The telescope is controlled by an Arduino mini-computer and star finding is done by means of star map, coordinates, guide-scope, aligned laser pointer and readouts from RA and Dec encoders. The advantage of this home-built system is that the Arduino can be programmed to a very accurate 6th decimal place tracking speed.

Fig. 1 The interior of the Soniville Observatory.

The first step was to determine if the above equipment was suitable and an evening's meeting was arranged to evaluate this. An evening's testing early July 2018 satisfied José that an attempt could be made.

It was determined that a transit, within reach of the capabilities of the Soniville Observatory, was predicted for the evening of 28th July. The host star was the 7.67 magnitude HD189733A in Vulpecula. The planet discovered there named HD189733b, is Jupiter- sized, orbiting once every 2.2 Earth days at a distance of 3 m kms around its slightly less than Sun-sized parent star. A characteristic of this transit was that the dimming be of sufficient depth for basic backyard astronomy equipment to detect.

The dimming for a transit is expressed in *mmag* – i.e. in thousandths of a magnitude. The depth of the transit caused by this exoplanet is 28/1000ths of a magnitude. In the week prior to T-Day (Transit-Day), all equipment was thoroughly checked and tests were done to make sure that the focal reducer would not only significantly brighten the image, but that it would sufficiently broaden the Field-of-View to include a wider range of comparison stars as well.

The principle behind detecting an exoplanet transit is straightforward – measure the brightness of the host star as often as possible before, during and after the transit. For a 2 hour transit, this requires 4 hours of taking images about every 30 seconds. However, the transiting planet is not the only factor that affects the apparent brightness of its parent.

As the target rises in the sky, the air mass through which it travels lessens, thus allowing more light through. Changing ambient lighting conditions – especially city light pollution – affect the perceived brightness. Transient factors such as thin passing clouds block out some of the light. What is needed is a nearby reference brightness against which to compare the brightness of the target star. The above-mentioned factors affect all the stars surrounding the target, so what is important is to measure the changes in the target which do NOT exhibit in the surrounding stars. These relative changes can then confidently be attributed to the dimming caused by the exoplanet.
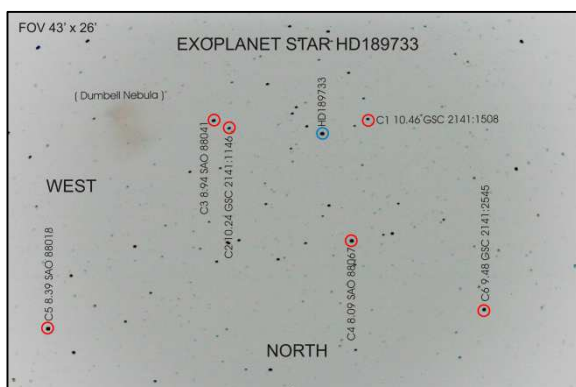
Fig. 2 *HD189733 (blue circle) other reference stars (red circles).*

Collecting photons in the CMOS sensor of the DSLR camera must be carefully done. It would be of no use to overfill the pixel buckets; saturating them means that data is

lost. Linearity is important – that is, it is important to know that collecting twice as many photons must show as double the voltage output from the sensor. Knowing how the sensor pixels respond to increasing numbers of collected photons is important so it was necessary to determine the optimum exposure settings to ensure that sufficient photons were filling the pixel bucket to reduce the inherent electronic noise in the camera well below the signal level generated by those incoming photons, this factor being known as the signal-to-noise ratio.

An hour before sunset flat fielding was started; this characterises the optics by taking images of the fading blue sky overhead and continually re-adjusting the exposure settings to ensure that at least 60% but not more than 80% of the photon capacity of the pixel buckets was being filled – this to ensure a decent enough signal-to-noise ratio without saturating. This process detects areas on the optical field where light transmission may be slightly reduced by dust particles and inhomogeneities in the lenses, mirrors and the camera sensor. By doing this, the sensitivity of each of the 12 million pixels in the camera sensor can be mathematically adjusted when analysing the images to cater for the inhomogeneities.

With the cap closing the telescope aperture, dark exposures were taken which characterise the electronic sensitivity of the individual camera pixels, after which bias frames were taken to determine how much noise is included in the overall voltage output from each pixel. The point of these procedures is to be able separate the signal generated by light photons emanating from HD189733 from any signals generated by the electronics in the camera.

After the period of astronomical twilight had passed, finding HD189733 in the nearby bright moonlight proved challenging. This reduced the time for taking out-of-transit (OOT) images before the transit started and so the first images taken were at the predicted start of the transit. Thereafter, it was a matter of monitoring the images to ensure that the star field remained centred in the 1 degree wide field of view.

Such periodic errors that do occur do not prevent software from being able to realign images when stacking and it did not have any impact on the ability to capture images except that some of the images show short tracks if captured during the most accelerated parts of the periodic error. (The initial results of this observation did not exclude the images which showed tracks, but will be discarded when further refining the data.)

Data was captured on two similar laptops; that author's and José's and there were a few challenges in transferring data from one laptop the other, but by monitoring data as it came in indicated that that valid data was being captured.

After the 109 minute transit was over, baseline data (OOT) continued to be captured for another hour after which the final darks and biases were taken and closed the observatory at 00h30.

Conclusion

The following day José advised that the transit had been successfully recorded.
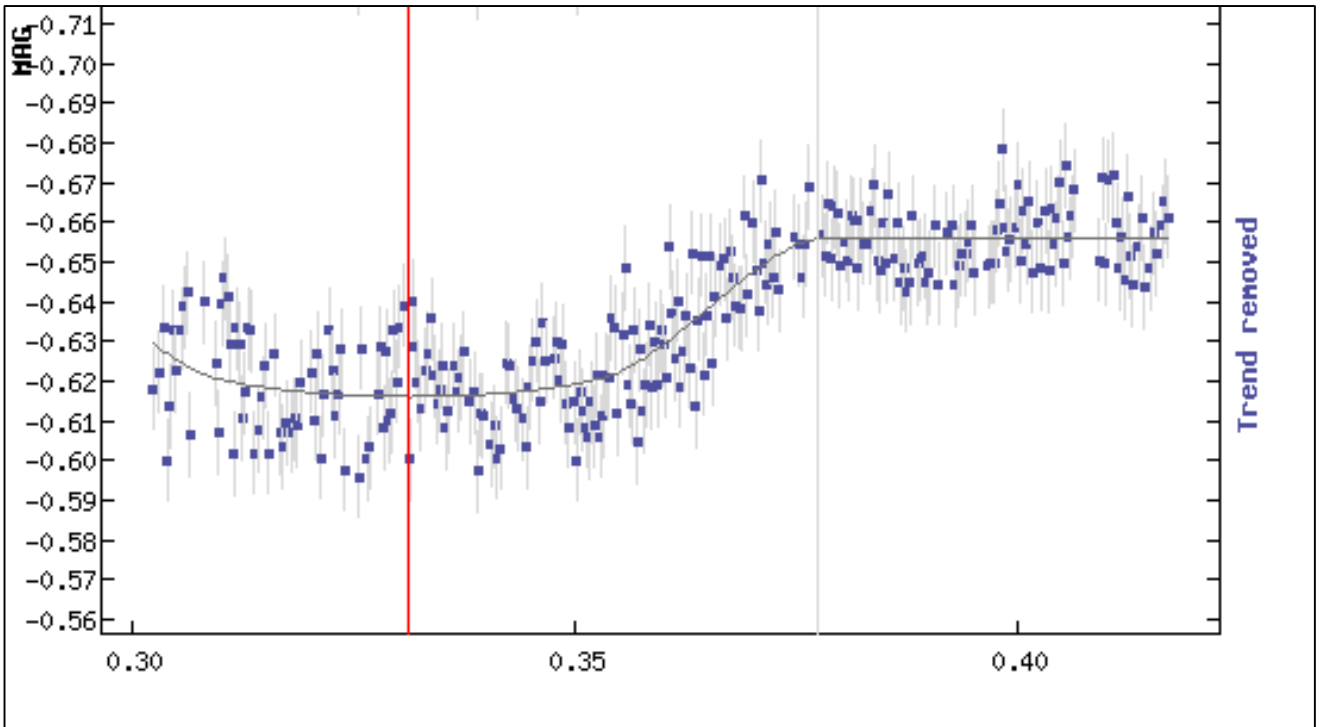
Fig. 3 *The magnitude indicated is instrumental magnitude (uncalibrated apparent magnitude). The analysis is done using differential photometry, so only the changes in the brightness are relevant. The X-axis labels are time expressed as a fraction of a Julian day, the day having been JD2458328, with mid-transit indicated by the red line.*

The raw data has been processed by a tool on the Exoplanet Transit Database http://var2.astro.cz/ETD/index.php. This process corrects for - amongst others - magnitude changes arising from changing atmospheric extinction as the observation elevation changed.

Since we were only able to start capturing shortly after the start of the transit, we do not have (OOT) measurements before the dip, as we do have after the dip. This inhibits the ability to determine the exact out-of-transit brightness.

The intention of these observations was to demonstrate that exoplanets could be observed using amateur equipment and DSLR's without expecting the data to be of

any scientific use. However we hope to improve on the data analysis and get it to a point where the data does have some scientific value but this may take some time.

The raw data is noisy but will continue to be refined in the future. We have to decide which software is most appropriate for amateur processing of photometric and particularly of exoplanet transit data.

Annual Index, Vol. 77 (2018)

ASSA Annual General Meeting 2018

Colloquia and Seminars

Sky Delights (Magda Streicher)

The **Astronomical Society of Southern Africa** (ASSA) was formed in 1922 by the amalgamation of the Cape Astronomical Association (founded 1912) and the Johannesburg Astronomical Association (founded 1918). It is a body consisting of both amateur and professional astronomers.

Publications: The Society publishes its electronic journal, the *Monthly Notes of the Astronomical Society of Southern Africa (MNASSA)* bi-monthly as well as the annual *Sky Guide Africa South.*

Membership: Membership of the Society is open to all. Potential members should consult the Society's web page assa.saao.org.za for details. Joining is possible via one of the local Centres or as a Country Member.

Local Centres: Local Centres of the Society exist at Bloemfontein, Cape Town, Durban, Hermanus, Johannesburg, Natal Midlands, Pretoria and Sedgefield district (Garden Route Centre). Membership of any of these Centres automatically confers membership of the Society.

Sky & Telescope: Members may subscribe to Sky & Telescope at a significant discount (proof of membership is required). Please contact the Membership Secretary for details.

Internet contact details: email: assa@saao.ac.za Home Page: http://assa.saao.ac.za

Council Members 2018		
President	Case Rijsdijk	particles@mweb.co.za
Vice-President	Dr Pierre de Villiers	pierredev@hermanusco.za
Vice-President	Chris Stewart	mwgringa@mweb.co.za
Membership Secretary	Wilmi Nel	assa@ipsissimaverba.co.za
Treasurer	AJ Nel	assa@ajnel.co.za
Secretary	Lerika Cross	lerika@icon.co.za
Scholarships	Dr Claire Flanagan	Claireflan55@gmail.com
Members	Clyde Foster	clyde@icon.co.za
	Dr Ian Glass	glass.ian@gmail.com
Bloemfontein Chair	Prof Matie Hoffman	HoffmaMJ@ufs.ac.za
Cape Chair	Eddy Nijeboer	Eddy47@xsinet.co.za
Durban Chair	Piet Strauss	pstrauss@marine-images.co.za
Garden Route Chair	Case Rijsdijk	particles@mweb.co.za
Hermanus Chair	Dr Pierre de Villiers	pierredev@hermanus.co.za
Johannesburg Chair	Jerome Jooste	astronomersinc@hotmail.co.za
Midlands Chair	Steffan Devos	sdevos@webbis.co.za
Pretoria Chair	Johan Smit	johanchsmit@gmail.com
Section Directors		
A - Shallow Sky	Clyde Foster	clyde@icon.co.za
B1 - Deep Sky B2 – Double and Variable Stars	Douglas Bullis Dave Blane	douglasbullis@gmail.com theblanes@telkomsa.net
C - Photometry, Spectroscopy	Percy Jacobs	percymj@iafrica.com
D - Cosmology/Astrophysics	Bruce Dickson	noisejammer@gmail.com
E - History	Chris de Coning	Siriusa@absamail.co.za
F - Dark Sky	Vacant	
G - Imaging	Martin Heigan	mheigan@icon.co.za
H – Instrumentation and ATM	Chris Stewart	mwgringa@mweb.co.za
I – Citizen Science	Allen Versfeld	Allan.versfeld@gmail.com

CONTENTS